Atmospheric composition and climate impacts of a future hydrogen economy

Nicola J. Warwick[1,2], Alex T. Archibald[1,2], Paul T. Griffiths[1,2], James Keeble[1,2], Fiona M. O'Connor[3,4], John A. Pyle[1,2] and Keith P. Shine[5]

[1]Department of Chemistry, University of Cambridge, Cambridge, CB2 1EW, UK
[2]National Centre for Atmospheric Science (NCAS), University of Cambridge, UK
[3]Met Office Hadley Centre, Exeter, UK
[4]Department of Mathematics and Statistics, Global Systems Institute, University of Exeter, UK
[5]Department of Meteorology, University of Reading, Reading, RG6 6ET, UK

Correspondence to: Nicola J. Warwick (Nicola.Warwick@atm.ch.cam.ac.uk)

Abstract. Hydrogen is expected to play a key role in the global energy transition to net zero emissions in many scenarios. However, fugitive emissions of hydrogen into the atmosphere during its production, storage, distribution and use could reduce the climate benefit and also have implications for air quality. Here we explore the atmospheric composition and climate impacts of increases in atmospheric hydrogen abundance using the UKESM1 chemistry-climate model. Increases in hydrogen result in increases in methane, tropospheric ozone and stratospheric water vapour, resulting in a positive radiative forcing. However, some of the impacts of hydrogen leakage are partially offset by potential reductions in emissions of methane, carbon monoxide, nitrogen oxides and volatile organic compounds from the consumption of fossil fuels. We derive a refined methodology for determining indirect Global Warming Potentials using parameters derived from steady-state simulations which is applicable to both shorter-lived species and those with intermediate and longer lifetimes, such as hydrogen. Using this methodology, we determine a 100-year Global Warming Potential for hydrogen of 12 ± 6. Based on this GWP and hydrogen leakages rates of 1 and 10%, we find that hydrogen leakage offsets approximately 0.4 and 4% respectively of total equivalent CO_2 emission reductions in our global hydrogen economy scenario. To maximise the benefit of hydrogen as an energy source, emissions associated with hydrogen leakage and emissions of the ozone precursor gases need to be minimised.

1 Introduction

The adoption of low carbon hydrogen (H_2) as an energy source could lead to substantial reductions in carbon dioxide emissions and a significant climate benefit. However, increasing levels of hydrogen in the atmosphere as a result of fugitive emissions from a hydrogen economy will affect atmospheric composition (e.g. Prather, 2003). It is important that the atmospheric implications of potential changes to hydrogen emissions are investigated in detail before the implementation of widespread hydrogen use.

The hydrogen abundance in the atmosphere increased over the twentieth century (Patterson et al., 2021), and today has a mixing ratio of around 530 parts per billion (ppb), with a small inter-hemispheric gradient (±20 ppb) (Novelli et al, 1999, Patterson et al., 2021). Fossil fuel combustion and biomass burning account for approximately 50% of the current total global hydrogen source, with the remainder arising from the oxidation of methane (CH_4) and volatile organic compounds (VOCs) in the atmosphere (e.g. Ehhalt and Rohrer 2009; Pieterse et al., 2013; Grant et al., 2010). Hydrogen removal is dominated primarily by uptake to soils and reaction with hydroxyl radicals (OH). OH is the main atmospheric oxidising agent and if hydrogen emissions were to increase, subsequent changes in the OH concentration could alter the lifetimes of important atmospheric greenhouse gases. Therefore, whilst hydrogen itself is not radiatively active, it can act as an indirect greenhouse gas.

An increase in the tropospheric concentration of hydrogen reduces the availability of OH via reaction R1. Reductions in tropospheric OH will result in increases in the atmospheric lifetime of CH_4 and its abundance (Derwent et al., 2001; Schultz et al., 2003; Warwick et al. 2004; Derwent et al., 2020; Derwent and Field 2021) since the major atmospheric sink of CH_4 is through reaction with OH (R2).

$$H_2 + OH \rightarrow H_2O + H \qquad \text{(R1)}$$

$$CH_4 + OH \rightarrow CH_3 + H_2O \qquad \text{(R2)}$$

The oxidation of both hydrogen and CH_4 in the troposphere can lead to the generation of ozone, with impacts for both climate and air quality (e.g., Archibald et al., 2020a; Schultz et al. 2003). In the stratosphere, oxidation of hydrogen and methane will lead to increases in stratospheric water vapour with potential implications for climate and stratospheric ozone (e.g., Tromp et al. 2003; Warwick et al., 2004). Increases in atmospheric hydrogen could also influence stratospheric ozone recovery through the production of HO_x radicals (=OH+HO_2), which are involved in ozone destruction cycles.

The extent to which future changes in hydrogen might affect atmospheric composition and climate will depend upon the level of hydrogen leakage and the ultimate size of a future hydrogen economy. In addition, emission reductions in species currently emitted by the production and consumption of fossil fuels, including methane, CO, NO_x (=NO+NO_2) and Volatile Organic Compounds (VOCs), will also induce feedbacks on atmospheric composition (e.g., Jacobson et al. 2008). There is significant uncertainty in the size of a future hydrogen economy and the leakage rates and emission reductions in other species are uncertain, depending on the forms of new technology implemented (e.g., Frazer-Nash 2022; Lewis 2021).

Here we report on calculations with the UKESM1 (Sellar et al., 2019) chemistry-climate model on the climate and atmospheric composition effects of a range of different atmospheric hydrogen boundary conditions, consistent with a range of different

scenarios for a future hydrogen economy. The work presented here is both based on, and an extension of, the work presented in Warwick et al., (2022). We determine changes in effective radiative forcing (ERF) and present an improved estimate of the hydrogen Global Warming Potential (GWP), accounting for composition changes in both the troposphere and stratosphere. As part of our GWP calculations, we present a refined methodology for calculating indirect GWPs from steady-state simulations, appropriate for use with both short-lived and longer-lived species.

2 Model and scenarios

2.1 The UK Earth System Model (UKESM1)

The U.K. Earth System Model, UKESM1 (Sellar et al., 2019), is a state-of-science Earth system model that couples Earth system modules to the HadGEM3-GC3.1 climate model (Kuhlbrodt et al., 2018; Williams et al., 2018). UKESM1 has a horizontal resolution of 1.875˚ in longitude and 1.25˚ in latitude, and 85 vertical levels extending from the surface to 85 km. Atmospheric composition changes are calculated using the UK Chemistry and Aerosols (UKCA) atmospheric chemistry module, which includes a coupled stratospheric-tropospheric chemistry scheme (Archibald et al., 2020b) and interactive 2-moment aerosol scheme (Mulcahy et al., 2020). UKCA includes the emissions of nine chemical species: nitric oxide (NO), carbon monoxide (CO), formaldehyde (HCHO), ethane (C_2H_6), propane (C_3H_8), acetaldehyde (MeCHO), acetone (Me_2CO), isoprene (C_5H_8) and methanol (MeOH), while surface mixing ratios of CH_4, N_2O, CFC-11 ($CFCl_3$), CFC-12 (CF_2Cl_2), CH_3Br, H_2 and COS are prescribed. The photochemical sources and sinks of H_2 (and CH_4) are fully interactive, but the use of the Lower Boundary Condition (LBC) fixes the atmospheric burden of H_2 (and CH_4). LBCs are widely used in chemistry-climate models as they 1) allow the observed burdens of intermediate lifetime (t>1 year) species to be imposed, bypassing the need to include emissions, and 2) remove the need for a long spin up for longer lived species burdens to reach a steady state. By using a LBC any chemical feedbacks that would affect the burden of these species are over-written. However, the effect of feedbacks on the steady state burden can be computed through quantification of the appropriate chemical feedback factors (see e.g., Heimann et al. (2020) for a discussion on how we have done this for methane).

2.2 Box model

Atmospheric box model simulations were performed using a coupled H_2-CH_4-CO-OH chemical scheme to link lower boundary condition values of H_2 with fugitive H_2 emission rates and obtain CH_4 lower boundary conditions for use in the UKESM1 experiments. In addition, the box model was used for extensive testing of the framework for GWP calculations.

Our box modelling approach is described in more detail in Warwick et al. (2022) and is similar to that described in Prather (1994) and used in other studies (Heimann et al., 2020; Nisbet et al., 2020). The model was initialised with realistic values for total methane emissions (585 Tg(CH_4) per year), CO (1300 Tg(CO) per year) and H_2 (80 Tg(H_2) per year) (e.g. Saunois et al., 2020; Pieterse et al., 2013; Zheng et al., 2019), and was found to give methane and H_2 levels in broad agreement with present

day levels – 1865 parts per billion (ppb) CH_4, 552 ppb H_2 and 101 ppb CO, as well as a CH_4 lifetime of 9.9 years, which is within the range of observationally-derived values.

2.3 Hydrogen economy scenarios

2.3.1 Changes in the abundance of atmospheric H_2 in a hydrogen economy

The increase in abundance of atmospheric H_2 in a future hydrogen economy is not well constrained due to uncertainties in fugitive emissions, which will depend on the ultimate size of the hydrogen economy and H_2 leakage rates, as well as uncertainties in the amount of H_2 undergoing uptake by soils. To guide our model scenarios, we estimate how emissions of H_2 and other species may change in response to a switch from fossil fuel to hydrogen technologies in an illustrative hydrogen economy scenario. In this scenario, approximately 23% of global energy consumption (about 133 EJ) is supplied by hydrogen (BP Energy Outlook, 2020). We here assume that 100% of the final energy consumption of fossil fuels in the buildings sector switches to hydrogen, along with 50% of the final energy consumption of fossil fuels in the transport sector and 10% of the final energy consumption of fossil fuels in the power generation sector. The lower percentages for transport and power generation reflect the smaller role hydrogen is assumed to play in these energy sectors due to the existence of low carbon alternatives such as electric vehicles and wind and solar power together with alternative storage options such as pumped hydro, batteries and compressed air (e.g. Staffell et al., 2019). New hydrogen technologies are assumed to have the same energy efficiency as the fossil fuel technology they are replacing (Staffell et al., 2019), except for in the transport sector where we assume diesel and petrol vehicles with an average tank-to-wheel energy efficiency of 30% will be replaced by vehicles using hydrogen fuel cells with an average efficiency of 50%. Using a net calorific value of 1 kg H_2 = 33.3 kWh, approximately 860 Tg H_2 yr^{-1} would be required to provide the energy consumption outlined above.

H_2 leakage rates from the infrastructure associated with a hydrogen economy are uncertain and will depend on many factors (e.g. E4tech, 2019). However, all else being equal, H_2 leakage rates are likely to be higher than for natural gas owing to the small molecule size of hydrogen. A recent study looking at the US natural gas supply chain indicated natural gas leaks of around 2.3% of gross gas production, which is ~60% higher than the US EPA inventory estimate (Alvarez et al., 2018). H_2 leakage rates of 1 and 10% (which represent the range of values used in previous studies e.g. Shultz et al. 2003, Warwick et al. 2004), would lead to additional H_2 emissions of 9 and 96 Tg H_2 yr^{-1} respectively based on a hydrogen economy supplying 23% of total present day energy consumption.

We bypass some of the uncertainty in H_2 leakage rates, the ultimate size of the hydrogen economy and soil uptake rates, by performing a range of hydrogen economy scenarios with fixed H_2 lower boundary mixing ratios. We consider scenarios with H_2 lower boundary conditions ranging from 500 to 2000 ppb (i.e. increases relative to present day mixing ratios of 0 to 1500 ppb), which we believe span much of these uncertainties (see Table 1). For example, based on the size of a hydrogen economy

outlined above, and assuming the magnitude of the soil sink increases in line with the increase in H_2 mixing ratios (i.e. a constant deposition velocity), box model simulations indicate H_2 lower boundary conditions of 750, 1000 and 1500 ppb represent H_2 leakage rates of about 3, 7 and 13% respectively (see Section 2.2 for further details on the box modelling). However, these H_2 lower boundary conditions would also be consistent with other fractions of total energy supplied by H_2, alternative soil sink responses and H_2 leakage rates. Use of this range of H_2 lower boundary conditions provides a clear signal in the atmospheric response to increased H_2 mixing ratios relative to interannual variability, and allows us to explore the linearity of the atmospheric response to increasing H_2. Note that our 2000 ppb H_2 scenario should be considered an extreme end member designed to assess the linearity of the atmospheric response to increasing atmospheric H_2, rather than a projection of potential future atmospheric H_2 levels in a hydrogen economy.

2.3.2 Changes in CH_4, CO, NO_x and VOC emissions in a hydrogen economy

To determine the associated changes in CH_4, CO, NO_x and VOC emissions, further assumptions are required about the new technology employed, in addition to the percentage of different energy sectors switching to H_2. In the buildings sector, we assume that H_2 will be combusted and NO_x emissions limited such that they remain unaltered (despite the potential for higher NO_x emissions from the increased flame temperature), whilst emissions of CH_4, CO and VOCs are eliminated. In the transport sector, we assume a 50% reduction in emissions of CH_4, CO, NO_x and VOCs based on 50% of oil-based transport being replaced by hydrogen fuel cells. In the power sector, we assume that stored hydrogen will be used to generate 30% of the electricity currently generated using natural gas via combustion and NO_x will remain unaltered, whilst emissions of CH_4, CO and VOCs are scaled appropriately. CH_4 emissions associated with energy production are also scaled according to the decreased use of CH_4 where it has been replaced by H_2. The assumptions above lead to reductions in CH_4, CO and NO_2 emissions of 43, 259 and 19 Tg yr^{-1} respectively (see Warwick et al. (2022) for further details).

Emission reductions for CO, NO_x and VOCs are determined by applying a uniform global scaling factor to emissions from the specific Gidden et al. (2019) energy sectors where hydrogen is assumed to play a role. The emission reductions determined for CH_4 are converted to a change in the CH_4 lower boundary condition for UKESM1 using the box model (see Section 2.2). To separate the atmospheric impacts of increasing hydrogen mixing ratios, the feedback on the CH_4 abundance and changes in the emissions of other species emitted by the consumption of fossil fuels, four different sets of hydrogen economy model simulations are performed as described in Table 1.

2.3.3 Model simulations

For the BASE simulation, all boundary conditions are taken from the recently developed CMIP6 dataset and we assume an H_2 LBC of 500 ppb. Climatological boundary conditions for sea surface temperatures, sea ice extent and anthropogenic and natural emissions are averaged over the years 2000-2014. In the first set of hydrogen economy scenarios, we consider changes to the atmospheric H_2 abundance only. In these simulations, the methane abundance is fixed at 1835 ppb (2014 year level), and does

not respond to changes in the methane lifetime. In the second set of hydrogen economy scenarios, we include the methane response to changes in atmospheric H_2 via the impact of H_2 on OH and the methane lifetime. The methane LBCs in these simulations are determined via a series of box model simulations where H_2 is varied (see Section 2.2). In the third set of hydrogen economy scenarios, we consider reductions in emissions of the ozone precursors CO, NO_x and VOCs from reduced fossil fuel use, whilst the methane abundance is fixed at 1835 ppb. The fourth set of hydrogen economy scenarios includes decreases in emissions of CH_4, CO, NO_x and VOCs from reduced fossil fuel use, in addition to the feedback of changes in the methane lifetime on the methane abundance. In these scenarios, we assume that all hydrogen will be green hydrogen, with no emissions of other species associated with the H_2 production method. In the case that blue or grey hydrogen is used, it is possible methane emissions may increase due to emissions occurring during hydrogen production (e.g. Bertagni et al., 2022). Each simulation was run for 40 years using annually repeating conditions, with the final 25 years of each simulation used for analysis and the initial 15 years treated as a spin-up period.

Hydrogen economy scenario	Experiment	H_2 LBC (ppb)	CH_4 LBC (ppb)	O_3 precursor emissions
Present day conditions	BASE	500	1835	2000-2014 climatology
Present day CH_4 and present day O_3 precursor emissions	750H2 1000H2 1500H2 2000H2	750 1000 1500 2000	1835	2000-2014 climatology
CH_4 feedback and present day O_3 precursor emissions	1500H2_CH4f 2000H2_CH4f	1500 2000	2058 2171	2000-2014 climatology
Present day CH_4 and reduced O_3 precursor emissions	500H2_O3pre 1500H2_O3pre 2000H2_O3pre	500 1500 2000	1835	CO, NO_x and VOC emissions reduced
CH_4 feedback and reduced O_3 precursor emissions	500H2_CH4f_O3pre 1000H2_CH4f_O3pre 2000H2_CH4f_O3pre	500 1000 2000	1652 1756 1961	CH_4, CO, NO_x and VOC emissions reduced

Table 1. List of UKESM1 hydrogen economy simulations employing different H_2 lower boundary conditions (LBCs). The CH_4 LBC used in the simulations not including a CH_4 feedback is 1835 ppb (2014 year level). In simulations including a CH_4 feedback (CH4f), the CH_4 LBC is determined using box modelling. Reductions in O_3 precursor emissions (O3pre) are described in Section 2.3.2.

3 Results

3.1 Atmospheric composition impacts following changes in hydrogen and methane

To determine the indirect radiative impact of hydrogen, we need to understand how CH_4, O_3 and H_2O will change, for unit emission of H_2. Those changes will depend not just on how H_2 changes, but also on changes in species from the production and use of fossil fuel. The scenario space is particularly complex and our scenarios should not be regarded as predictions. Instead, here we try to indicate generally how the composition of radiatively active species might change and which changes are linear in the change in H_2, looking first at the changes driven by H_2 and CH_4.

Figure 1 summarises the key composition changes seen for a range of different hydrogen lower boundary mixing ratios when emissions of other species from the fossil fuel industry are held constant (blue and red circles) and when they are reduced (orange and green circles). Decreases in OH, the main atmospheric oxidant, are modelled throughout the troposphere with larger decreases in scenarios with higher H_2 abundances (Figure 1a), consistent with R1 being the main atmospheric sink for H_2. The change in OH is linear in H_2 both when the surface CH_4 mixing ratio is held constant (blue circles) and when it is increased to account for the feedback of changes in OH on the methane abundance (red circles). When including this methane feedback, tropospheric mean OH decreases by about 0.90×10^5 molecules cm^{-3} (or about 10%) for every 1000 ppb (1 ppm) increase in H_2 (Figure 1a, red circles). These modelled changes in OH go on to cause a cascade of further composition changes by altering the methane lifetime, production and destruction rates of tropospheric ozone, as well as aerosol nucleation rates and cloud condensation nuclei (CCN) concentrations.

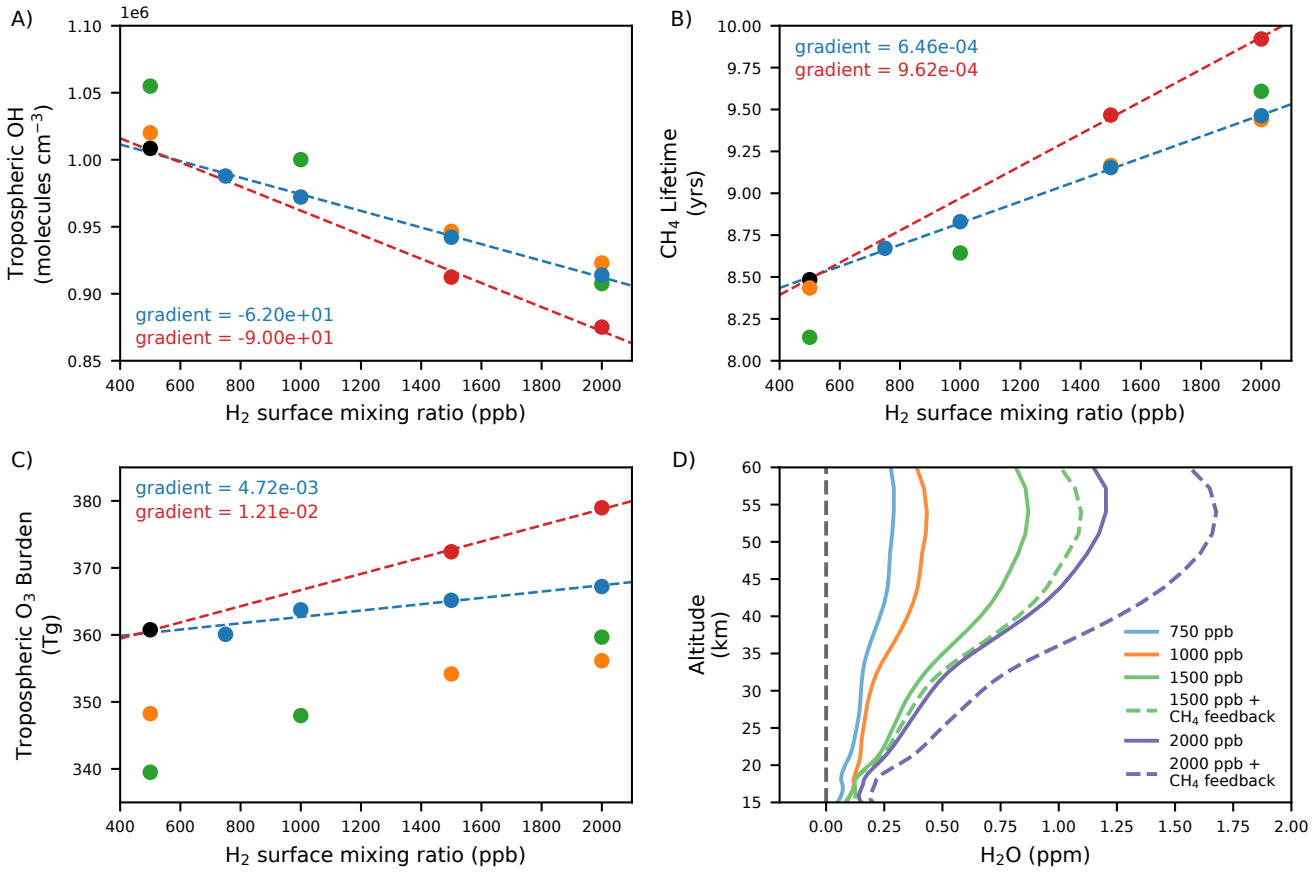

Figure 1. The response of (A) mass weighted tropospheric mean OH, (B) CH_4 lifetime with respect to OH, (C) tropospheric O_3 and (D) stratospheric water vapour to increasing H_2 mixing ratios in UKESM. In Figures 1A-C, the black circle represents the BASE scenario, blue circles represent scenarios where the CH_4 LBC remains fixed at 2014 levels, red circles are scenarios where the CH_4 LBC is adjusted to account for the change in CH_4 lifetime, orange circles are scenarios including changes in emissions of ozone precursors, and green circles include both changes to emissions of CH_4 and ozone precursors, as well as adjusted CH_4 LBCs to account for the response of the CH_4 abundance to changes in the CH_4 lifetime. The blue dashed line represents the fit through experiments where the CH_4 LBC remains fixed at 2014 levels, and the red dashed line is the fit through experiments which include the response of CH_4 to changing H_2 (and OH). Figure 1D shows the change in the vertical profile of H_2O relative to the BASE scenario where the H_2 LBC is increased to 750, 1000, 1500 and 2000 ppb. Solid lines represent scenarios where CH_4 is fixed at 2014 levels, whereas dashed lines show scenarios where the CH4 LBC is increased to account for the change in CH4 lifetime.

Figure 1b shows the CH_4 lifetime as a function of atmospheric H_2 and tropospheric OH. In the BASE simulation, the modelled CH_4 lifetime with respect to loss by reaction with tropospheric OH is 8.5 years. This value is lower than the range given for the total chemical methane lifetime in IPCC AR6 (9.7 ± 1.1 years, Forster et al., 2021), but comparable to a present day total chemical multi-model estimate of 8.4 ± 0.3 years in Stevenson et al. (2020) and in good agreement with the lifetime stimulated with our box model. As atmospheric H_2 increases but all other factors remain constant, there is a linear increase in the CH_4 lifetime. The methane lifetime increases by 0.64 years for every 1000 ppb (1 ppm) increase in H_2 when the methane abundance is held constant (blue circles), or 0.96 years for every 1000 ppb increase in H_2 when the methane abundance is increased in response to the modelled changes in its lifetime (red circles).

The oxidation of H_2 in the troposphere can also affect the levels of ozone (O_3) as the HO_2 produced through R1 can catalyse the interconversion of NO_x which drives tropospheric ozone production (e.g., as reviewed in Archibald et al., 2020a):

$$NO + HO_2 \rightarrow NO_2 + OH \qquad (R3)$$

followed by photolysis of NO_2 to form ozone

$$NO_2 + h\nu \rightarrow NO + O\ (+O_2 = O_3) \qquad (R4)$$

In addition, changes in OH and HO_2 produced via R1 influence the destruction of tropospheric ozone by altering the flux through the reaction of O_3 with both of these species. Overall, the tropospheric ozone burden increases approximately linearly with atmospheric H_2 increase, driven primarily through increases in the reaction HO_2 + NO (R3), which increases by ~7% when atmospheric H_2 increases to 2000 ppb (Figure 1c). Changes in the ozone budget are documented in Table S2.

Increased H_2 mixing ratios at the surface can also influence stratospheric composition. Increases in H_2 and CH_4 abundance in the troposphere result in an increased flux of these species to the stratosphere, where their oxidation leads to the production of water vapour. Figure 1d shows the increase in the stratospheric water vapour profile relative to the BASE scenario when tropospheric H_2 increases from 500 ppb to 750, 1000, 1500 and 2000 ppb, both where the tropospheric methane abundance remains unchanged, and where the methane LBC is adjusted in response to modelled changes in the methane lifetime. When H_2 increases to 2000 ppb, but CH_4 is held constant, stratospheric H_2O increases by up to 25% (> 1 ppm). If the tropospheric methane abundance is increased in line with modelled changes in the CH_4 lifetime, larger increases in stratospheric H_2O are simulated.

3.2 Atmospheric composition impacts when hydrogen, methane and ozone precursor emissions all change

The impacts discussed above arise from changes in atmospheric H_2 abundance and subsequent changes in methane abundance arising from the feedback of OH on the methane lifetime. Expected reductions in ozone precursor emissions of CO, NO_x (which may also increase locally), VOCs and CH_4 following a shift to a global hydrogen economy also have the potential to further impact atmospheric composition. The green and orange circles in Figures 1a-c show the impact of including these other emission changes, with and without the feedback on the methane abundance included respectively. The relationship remains linear for the airmass weighted tropospheric mean OH, methane lifetime and tropospheric ozone burden plotted as a function of H_2 LBC. In all cases, the gradients remain similar to the corresponding scenarios not including the ozone precursor emission reductions (note the ozone precursor emission changes are the same across all scenarios).

The linear relationships shown in Figure 1 allow the global methane and ozone changes for a range of different hydrogen economy scenarios to be estimated, giving the response to different realisations of a future hydrogen economy. They can also be employed to derive a GWP for hydrogen (see Section 3.4).

Some detail on geographical changes in tropospheric ozone in a hydrogen economy is provided in Figure 2. As the photochemical production of ozone is driven by oxidation of CO, CH_4 and VOCs in the presence of NO_x, the net regional change in ozone depends not only on how H_2 changes, but also on changes in emissions of these species. This sensitivity is demonstrated in Figure 2.

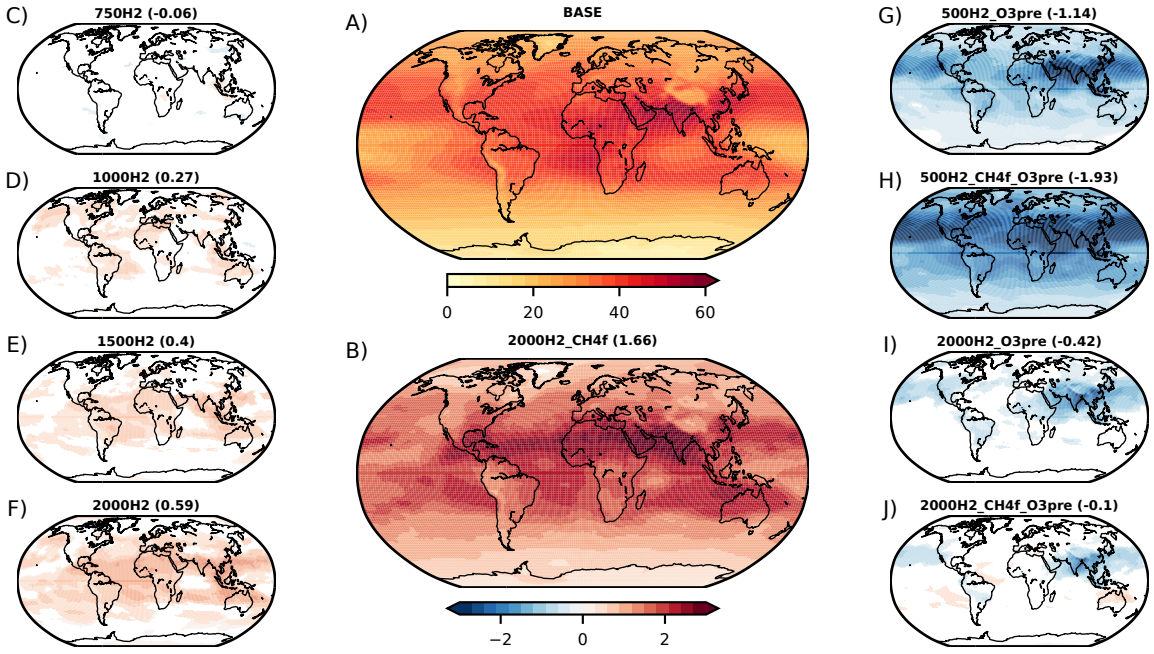

265 Figure 2. The effect of increases in atmospheric H_2 on tropospheric ozone column: (a) tropospheric ozone column for the BASE scenario (DU), (b) the change in tropospheric ozone column relative to BASE when H_2 is increased to 2000 ppb, including the response of the methane abundance to changes in the methane lifetime (DU), (c) to (f) changes in tropospheric ozone column relative to BASE when H_2 mixing ratios are increased, but all other factors including the methane abundance remain fixed, and (g) to (j) changes in tropospheric ozone column relative to BASE for scenarios including emission reductions
270 in ozone precursors and methane. The numbers above each figure give the change in global mean tropospheric column in DU relative to BASE; only differences that are statistically significant at the 95% confidence level are presented.

When H_2 increases, so does tropospheric ozone (Figures 2c to 2f, see also Figure 1c). Similarly, when atmospheric methane increases, the effect is to enhance the tropospheric ozone column increase (compare Figure 2b with Figure 2f. In contrast,
275 reductions in ozone precursor and CH_4 emissions would avoid the significant O_3 increases seen in Figure 2b (see Figures 2h and 2j). For example, if there is no H_2 leakage, reductions in the other emissions (Figure 2g and 2h) lead, as expected, to reductions in tropospheric ozone. When surface H_2 reaches 2000ppb, reductions in the other emissions still lead to modest decreases in ozone (Figures 2i, 2j). For example, in the UKESM1 simulation which assumes a large H_2 leakage, with surface mixing ratios of H_2 reaching 2000 ppb, and emissions reductions in CH_4, CO, NO_x, and VOCs, the global mean tropospheric
280 column ozone response is found to be small (-0.1 DU) due to the competing effects outlined above (Figure 2j). The tropospheric ozone response to a global shift towards a hydrogen economy is therefore strongly influenced by the amount of hydrogen added to the atmosphere through leaks, and the co-benefit reductions achieved in CO, NO_x, VOC and CH_4 emissions.

As shown above, the changes in H_2 and methane affect OH, which can in turn also influence aerosols in our model simulations. We simulate a linear decrease in tropospheric air mass weighted OH (Figure 1a), and thus the OH+SO_2 reaction flux, for increasing H_2 in the atmosphere. The reduction in the flux through the OH+SO_2 reaction results in a shift from oxidation of SO_2 in the gas phase (which contributes towards new particle formation) towards oxidation in the condensed phase (which grows existing particles). Such a shift leads to a reduction in the aerosol number and increase in aerosol size with impacts on clouds and radiative forcing (see O'Connor et al., 2022 for further details). The modelled decrease in OH following the increase in H_2 is coincident with an increase in HO_2 (R1 leads to the production of H atoms which in the troposphere near instantaneously form HO_2); thus, H_2 acts to increase the HO_2:OH ratio, similar to CO. We find that the HO_2:OH ratio linearly increases with increasing H_2 in the atmosphere (from 145 at 500 ppb H_2 to 175 at 2000 ppb H_2) and as a result the H_2O_2 concentration increases, further enhancing in-cloud oxidation of SO_2. Whilst our simulations demonstrate the potential importance of aerosol feedbacks relating to changes in OH, the inclusion of other aerosols, e.g. nitrates, may influence our results and more studies involving multiple models are required to constrain the uncertainties involved.

3.3 Effective radiative forcing

Figure 3 shows the effective radiative forcing (ERF) for the scenarios in Table 1. Our ERF values are based on the chemical changes in composition resulting from increases in atmospheric H_2, in addition to changes in emissions of CH_4, CO, NO_x and VOCs in the scenarios where these are included. The calculated ERFs do not include the large climate benefit expected from anticipated reductions in CO_2. We determined the ERF following Equation (8) from O'Connor et al. (2021). The ERF can also be decomposed into a clear-sky and a cloud radiative forcing, with the latter calculated from a change in the cloud radiative effect (CRE) from "clean" radiation calls that exclude aerosol-radiation interactions (Ghan, 2013). The clear-sky forcing, in principle, may include a contribution from aerosol-radiation interactions, but the magnitude of this contribution was found to be less than 0.02 W m^{-2}. The time-slice experiments using an atmosphere-only model, i.e. using decoupled sea surface temperature (SST) and sea-ice coverage, permit the determination of the top-of-atmosphere radiative forcing including rapid adjustments to cloud and water vapour. The ERF was calculated relative to the 2014 base case. The ERF varies from a cooling (negative ERF) to a warming (positive ERF) tendency depending on the scenario. The ERF increases with H_2 over the range 500 – 2000 ppb. Table 2 shows that these increases are due to both clear-sky and cloud radiative forcing. The clear-sky forcing increases with increasing H_2 presumably due to increased O_3, while the CRE can be ascribed to small decreases in cloud albedo. Figure 4 shows that increasing H_2 from 500 ppb to 2000 ppb leads to changes in cloud droplet number concentration (CDNC) across the globe. The decreased CDNC leads, for the same amount of water vapour, to larger cloud droplets and lower cloud albedo. This leads to a CRE of 0.05 Wm^{-2}. In scenarios where CH_4 is increased, the further suppression of OH leads to a stronger CRE. Whilst the radiative forcing from the CRE in our hydrogen economy scenarios increases the total ERFs by approximately 50%, thus forming a significant component of indirect forcing from H_2, we do not include forcing

315 from clouds in our GWP calculations. Such couplings between oxidants, aerosols and clouds are relatively unique in UKESM compared with other CMIP6 models and more studies are required to constrain the uncertainties involved.

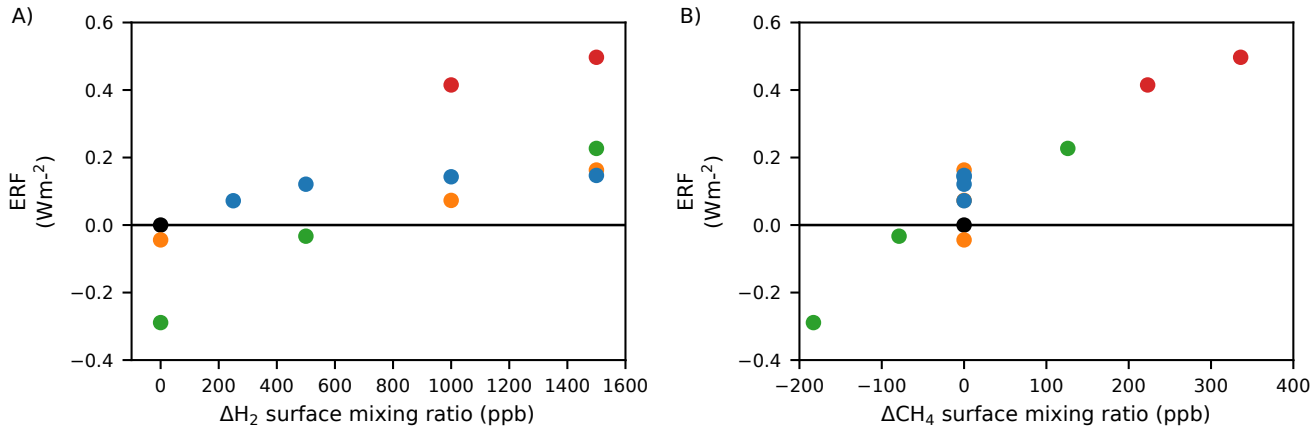

320

Figure 3. The effect of the simulated changes in atmospheric composition on effective radiative forcing (ERF). Left hand panel shows the ERF as a function of H_2 and other experimental conditions; right hand figure shows the ERF as a function of CH_4 and other experimental conditions. As for Figures 1a-c, the black circle represents the BASE scenario, blue circles represent scenarios where the CH_4 LBC remains fixed at 2014 levels, red circles are scenarios where the CH_4 LBC is adjusted to account
325 for the change in CH_4 lifetime, orange circles are scenarios including changes in emissions of ozone precursors, and green circles include both changes to emissions of CH_4 and ozone precursors, as well as adjusted CH_4 LBCs to account for the response of the CH_4 abundance to changes in the CH_4 lifetime. Note that none of the calculated ERFs include anticipated reductions in CO_2.

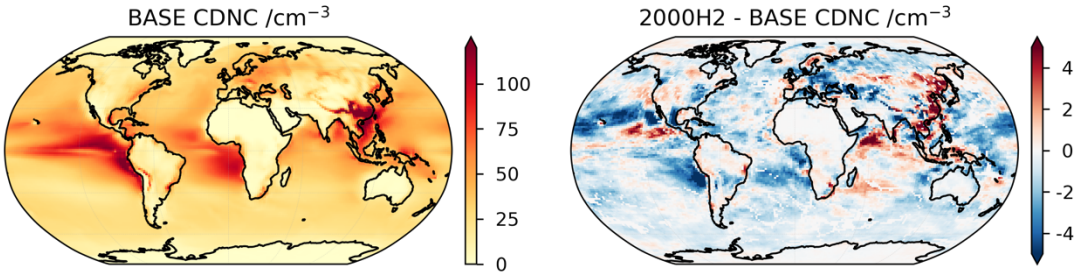

Figure 4. Cloud droplet number concentration (CDNC) in the UKESM1 model at 1 km altitude. The left hand figure shows CDNC in the BASE (500 ppb H_2) scenario, the right hand the change in CDNC when H_2 is increased to 2000 ppb (2000H2 scenario).

Hydrogen economy simulation	LW Clear Sky	SW Clear Sky	Net Clear Sky	LW Cloud Radiative Effect	SW Cloud Radiative Effect	Net Cloud Radiative Effect	Net ERF
750H2	0.06 ± 0.03	0.01 ± 0.03	0.06 ± 0.03	-0.02 ± 0.02	0.03 ± 0.02	0.01 ± 0.02	0.08 ± 0.04
1000H2	0.04 ± 0.03	0.03 ± 0.02	0.07 ± 0.03	-0.05 ± 0.02	0.09 ± 0.03	0.04 ± 0.03	0.10 ± 0.05
1500H2	0.09 ± 0.03	0.02 ± 0.02	0.07 ± 0.03	-0.03 ± 0.02	0.10 ± 0.03	0.07 ± 0.03	0.15 ± 0.04
2000H2	0.09 ± 0.02	0.00 ± 0.02	0.09 ± 0.03	-0.04 ± 0.02	0.10 ± 0.04	0.06 ± 0.03	0.15 ± 0.04
1500H2_CH4f	0.19 ± 0.03	0.06 ± 0.02	0.25 ± 0.03	-0.10 ± 0.01	0.19 ± 0.04	0.09 ± 0.03	0.34 ± 0.05
2000H2_CH4f	0.29 ± 0.03	0.06 ± 0.02	0.36 ± 0.03	-0.15 ± 0.01	0.30 ± 0.03	0.16 ± 0.03	0.51 ± 0.04
500H2_O3pre	0.00 ± 0.03	0.00 ± 0.02	0.00 ± 0.02	0.00 ± 0.02	-0.05 ± 0.03	-0.05 ± 0.03	-0.05 ± 0.04
1500H2_O3pre	0.07 ± 0.03	-0.01 ± 0.02	0.06 ± 0.03	-0.04 ± 0.02	0.08 ± 0.03	0.05 ± 0.03	0.10 ± 0.05
2000H2_O3pre	0.08 ± 0.03	0.03 ± 0.02	0.10 ± 0.03	-0.01 ± 0.02	0.07 ± 0.03	0.06 ± 0.03	0.16 ± 0.04

500H2_CH4f_O3pre	-0.13 ± 0.03	-0.03 ± 0.02	-0.15 ± 0.03	0.11 ± 0.02	-0.20 ± 0.03	-0.09 ± 0.03	-0.24 ± 0.05
1000H2_CH4f_O3pre	0.00 ± 0.02	-0.04 ± 0.02	-0.04 ± 0.03	0.05 ± 0.02	-0.06 ± 0.03	-0.01 ± 0.03	-0.05 ± 0.04
2000H2_CH4f_O3pre	0.13 ± 0.03	0.03 ± 0.02	0.16 ± 0.03	-0.09 ± 0.02	0.15 ± 0.04	0.06 ± 0.03	0.22 ± 0.05

Table 2. ERFs and their clear-sky and cloud radiative effect components in the shortwave (SW) and longwave (LW) calculated using the method outlined in Ghan (2013) (as used in O'Connor et al., 2021; 2022), based on the last 30 years of the hydrogen simulations. All units are in W m^{-2}.

340

3.4 Global Warming Potential

A GWP quantifying the indirect radiative forcings associated with H_2 has so far only previously been determined in a very limited number of studies including Derwent et al., (2020) (an update on Derwent et al., 2006), Field and Derwent, (2021), Hauglustaine et al. (2022), and Sand et al. (2023). The first two studies considered only the influence of H_2 on tropospheric
345 composition, whereas Hauglustaine et al. (2022) and Sand et al. (2023) included both the tropospheric and stratospheric response. In addition to these studies, Ocko and Hamburg (2022) extended the work presented in Warwick et al. (2022) to calculate hydrogen's GWP for a range of time horizons.

We determine a GWP for H_2 based on composition changes in both the troposphere and stratosphere in our UKESM1
350 simulations, using radiative forcing scaling factors from Myhre et al., (2013) and Forster et al. (2021) and the equations E1 to E4 presented in Section 3.4.1 (see also Warwick et al., (2022)). Our new estimate of the H_2 GWP considers changes in methane and ozone in the troposphere, as well as changes in stratospheric water vapour and stratospheric ozone. Note that we have not used the model-derived ERFs from Section 3.3 in the GWP calculations below. The model-derived ERFs (for H_2 leakage only, including the methane response) are larger than the radiative forcing due to hydrogen determined from modelled changes in
355 chemical composition using radiative forcing scaling factors from Forster et al. (2021) (see Section 3.4.2). Much of this difference arises due to the large contribution from clouds to the model-based ERFs (see Table 2) that is not accounted for in the radiative forcing scaling factors. For our GWP calculations, we determine the radiative forcing using the modelled changes in composition along with the radiative forcing scaling factors rather than the ERFs. Our reason for this is two-fold. Firstly, it ensures the large uncertainty associated with the aerosol-cloud component of the ERFs (Forster et al., 2021) is not propagated
360 into the GWP calculations. Secondly, significant further work would be required to attribute the calculated total ERFs to individual species, so that the appropriate lifetimes could be applied to the different components of the forcing that contribute to the GWP. However, we note that if the model ERFs were to be used in the GWP calculations, the GWPs presented in the next section would be larger.

3.4.1 Methodology

For our GWP calculation, we derive a more universal version of the approach presented in Fuglestvedt et al. (2010) for calculating GWPs for species whose emissions result in indirect radiative forcings, which was also implicitly adopted for Global Temperature Change Potentials in the IPCC Sixth Assessment Report (Forster et al., 2021). The Fuglestvedt et al. (2010) method assumes that the time evolution of the radiative forcing depends only on the lifetime of the species causing the forcing and not the lifetime of the species being emitted. In their method, the time evolution of the radiative forcing during a one-year constant emission is described by an approach to steady-state with a time constant according to the lifetime of the species causing the forcing. The peak forcing is assumed to occur directly at the end of the one-year emission, and subsequently to decay with the same lifetime as in the growth phase. Although this assumption may be a good approximation for short-lived emission species such as NO_x, it may not be for species with longer lifetimes such as H_2. Our extension of their method (see Warwick et al., 2022) accounts for both the lifetime of the emitted species and the lifetime of the species causing the forcing; it also allows the time period of the constant emission to be varied. The use of a one year constant emission rather than an emission pulse has the benefit of removing the time of year dependence of when the emission pulse occurs.

In our method for deriving indirect GWPs from steady-state simulations, we include the indirect forcing due to perturbations in radiatively active species arising (a) during the constant emission (AGWP1, E1), (b) from the decay of the perturbation subsequent to the end of the constant emission (AGWP2, E2) and (c) perturbations arising from the emission species remaining in the atmosphere after the end of the constant emission (AGWP, E3). Derivations for E1 to E3 are presented in Appendix 1.

$$AGWP1 = \frac{R\ a_M \alpha_M \alpha_H C}{t_p}\left(tp - \alpha_M\left(1 - exp\left(\frac{-t_p}{\alpha_M}\right)\right) - \left(\frac{\alpha_H}{\alpha_H - \alpha_M}\right)\left(\alpha_H\left(1 - exp\left(\frac{-t_p}{\alpha_H}\right)\right) - \alpha_M\left(1 - exp\left(\frac{-t_p}{\alpha_M}\right)\right)\right)\right) \quad \text{(E1)}$$

$$AGWP2 = \frac{\left(R\ a_M \alpha_H^{\,2}\ \alpha_M\ \mathrm{C}\left(1 - \exp\left(\frac{-t_p}{\alpha_H}\right)\right)\right)}{t_p\ (\alpha_H - \alpha_M)}\left(\alpha_H\left(1 - \exp\left(-\frac{(Hz - t_p)}{\alpha_H}\right)\right) - \ \alpha_M\left(1 - \exp\left(-\frac{(Hz - t_p)}{\alpha_M}\right)\right)\right) \quad \text{(E2)}$$

$$AGWP3 = \frac{R\ a_M \alpha_M^2 \alpha_H\ \mathrm{C}}{t_p}\left(\left(1 - \exp\left(-\frac{t_p}{\alpha_M}\right)\right) - \left(\frac{\alpha_H}{\alpha_H - \ \alpha_M}\right)\left(\exp\left(-\frac{t_p}{\alpha_H}\right) - \exp\left(-\frac{t_p}{\alpha_M}\right)\right)\right)\left(1 - \exp\left(-\frac{(Hz - t_p)}{\alpha_M}\right)\right) \quad \text{(E3)}$$

Where:

$AGWP$ = absolute global warming potential (W m^{-2} kg^{-1} yr)

M = species resulting in the indirect radiative forcing: CH_4, O_3 and H_2O (ppb or DU for tropospheric O_3)

R_M = radiative forcing efficiency for M (W m^{-2} ppb^{-1} or W m^{-2} DU^{-1} for tropospheric O_3)

a_M = production rate of M [ppb yr^{-1}] per ppb H_2 change at steady-state (yr^{-1})

α_M= Atmospheric lifetime of M (yr)

α_H = Atmospheric H_2 lifetime (combined chemical and deposition lifetime) (yr)

Hz = the time horizon considered (yr)

C = conversion factor for converting H_2 mixing ratio (ppb) into H_2 mass (kg)

t_p = length of step emission (yr)

Equations E1 to E3 are applied separately to methane and non-methane-induced ozone and stratospheric water vapour to calculate a net GWP for H_2. The associated indirect GWPs for each radiative species perturbed by hydrogen are then given by:

$$GWP_{H2} = \frac{AGWP_{H2}}{AGWP_{CO2}} \quad \text{(E4)}$$

A comparison of the time evolution of the methane perturbation resulting from a change in H_2 mixing ratio based on the standard Fuglestvedt et al. (2010) equations and our updated equations is shown in Figure 5. Accounting for the atmospheric lifetime of hydrogen in the updated equations results in a slower predicted rate of increase in methane during the one-year constant emission relative to the standard Fuglestvedt et al. (2010) equations, a delayed methane peak (peaking at 5 years rather than 1 year, using the parameters specified in the caption) and a slower rate of methane decrease subsequent to that peak; as methane is still being impacted by the remaining H_2. This difference occurs as the equations from Fuglestvedt et al. (2010) assume that the emitted species instantaneously reaches a new steady-state atmospheric concentration at the start of the one-year constant emission. In addition, their assumption that the decay following the peak forcing is controlled only by the lifetime of the radiatively active species neglects any subsequent perturbations to atmospheric chemistry as a result of the emitted species still present in the atmosphere after the end of the one-year constant emission. A comparison of the transient methane growth due to an H_2 perturbation as determined by equations E1 to E3 in Figure 5 (grey line) with model studies where methane has been free-to-respond to an H_2 perturbation (including the box model described in Section 2.2 and the model studies of Derwent et al., 2020 and Bertagni et al., 2022) shows that the response represented by equations E1 to E3 is similar to that found in transient model simulations following an H_2 pulse emission.

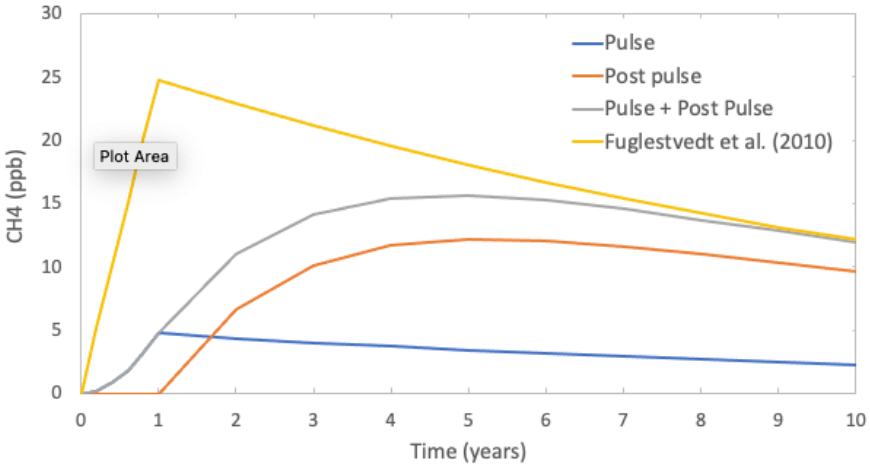

Figure 5. The time evolution of excess methane during and after a one year step hydrogen emission (based on a steady-state H_2 excess of +1500 ppb, an H_2 lifetime of 1.96 years and a methane perturbation lifetime of 11.8 years) as predicted by the Fuglestvedt et al. (2010) equations (yellow) and our updated equations. For our updated equations, the excess methane is split into contributions from methane generated during the step emission (blue), methane generated from excess hydrogen remaining in the atmosphere after the one year step emission (orange), with the total methane excess shown in grey.

Equations E1 to E3 are derived using a framework assuming a one year constant emission rather than an emission pulse. This has the benefit of removing the time-of-year dependence of the atmospheric perturbations arising from the emission pulse. However, once derived, the chemical parameters from our UKESM simulations can also be applied to the pure pulse approach with little error. Equations E1 to E3 can be simplified by taking the $t_p \rightarrow 0$ limit of equation E2, which is given in equation E5. Based on our derived parameters, using equation E5 rather than equations E1 to E3 leads to a difference of 0.1% for our hydrogen GWP(100) and 1.5% for our hydrogen GWP(20). In contrast, using the original method of Fuglestvedt et al. (2010) leads to a 0.1% difference in our hydrogen GWP(100), but a 5% difference in our hydrogen GWP(20) relative to equations E1 to E3.

$$AGWP = \frac{R\, a_M \alpha_H\, \alpha_M\, \mathrm{C}}{(\alpha_H - \alpha_M)} \left(\alpha_H \left(1 - \exp\left(-\frac{Hz}{\alpha_H}\right)\right) - \alpha_M \left(1 - \exp\left(-\frac{Hz}{\alpha_M}\right)\right)\right) \quad \text{(E5)}$$

3.4.2 Calculation of a hydrogen GWP

In our calculations, $AGWP_{CO2}(100)$ and $AGWP_{CO2}(20)$ are taken to be 9.17×10^{-14} (± 26%) and 2.49×10^{-14} (± 18%) W m^{-2} kg^{-1} yr (Myhre et al., 2013) respectively. $AGWP_{H2}$ is taken as the sum of AGWP1-3. The values for $AGWP_{CO2}$ (100) and

$AGWP_{CO2}(20)$ change slightly to $8.95x10^{-14}$(± 26%) and $2.43x10^{-14}$(± 18%) W m^{-2} kg^{-1} yr in Forster et al. (2021): the impact of this on our H_2 GWP calculation, along with other IPCC AR6 (Forster et al., 2021) updates, is shown in Table 3. The length of the step emission, t_p, is 1 year, Hz is taken to be 20 or 100 years and a_H is 1.96 years (with an uncertainty range from 1.4 to 2.2 years). The conversion factor, C, for converting H_2 mixing ratio into H_2 mass based on UKESM1 data is $3.52x10^{-9}$ ppb kg^{-1}. Values for R_M, a_M, and α_M are dependent on the species causing the indirect forcing (methane, ozone and stratospheric water vapour).

For methane, R_{CH4} is taken to be 0.000363 (±10%) W m^{-2} (ppb CH_4)$^{-1}$ (Myhre et al., 2013) or 0.000389 W m^{-2} (ppb CH_4)$^{-1}$ (Forster et al., 2021). The methane perturbation lifetime, α_{CH4}, in UKESM1 is derived to be 11.8 years in this study, which falls within the range given by IPCC AR5 (12.4 ± 1.4 years, Myhre et al., 2013). The value for a_{CH4}, an additional methane production rate term per unit increase in H_2, represents the positive CH_4 tendency resulting from an increase in H_2 and corresponding decrease in OH and is defined as:

$$a = CH_4\, k_{CH4+OH}\, \frac{dOH}{dH_2}$$

where CH_4 is the methane lower boundary condition (1835 ppb in UKCA), k_{CH4+OH} is the global mean airmass-weighted rate constant for the reaction of CH_4 with OH and dOH/dH_2 is the rate of change of OH with respect to H_2. Values for these parameters derived from UKESM1 simulations are as follows: $k(CH_4 + OH)$ = $2.8x10^{-15}$ cm^3 $molecule^{-1}$ s^{-1}, dOH/dH_2 = $3.68x10^{-9}$ (dimensionless). $k(CH_4 + OH)$ is determined from the gradient of methane lifetime against 1/(global airmass-weighted mean OH), and dOH/dH_2 from the gradient of the mass-weighted tropospheric mean OH concentration against H_2 surface mixing ratio for the UKESM1 simulations including the feedback on the methane lifetime via an adjusted CH_4 lower boundary condition determined by the box model (see Figure 1a). It is also possible to derive dOH/dH_2 using the gradient of the mass-weighted tropospheric mean OH concentration against H_2 surface mixing ratio from the UKESM1 simulations where only the H_2 LBC is varied (whilst the CH_4 LBC is held constant) in combination with the equation below from Stevenson et al. (2013), and the methane feedback factor with respect to OH only of 1.49 derived for UKESM1,

$$CH_{4\,new} = CH_{4\,base}\left(\frac{\tau_{new}}{\tau_{base}}\right)^f$$

where f is the methane feedback factor, $CH_{4\,base}$ and τ_{base} are the lower boundary condition and chemical lifetime for methane in the base scenario, and $CH_{4\,new}$ and τ_{new} are the lower boundary condition and chemical lifetime for methane in the perturbed H_2 scenarios. The difference between the dOH/dH_2 values derived using the two methods above is approximately 2% (or 3% if using the methane feedback factor of 1.39 derived with respect to all sinks). This in turn leads to a 2% difference in the methane-induced hydrogen GWP terms and a difference of less than 1% in the total hydrogen GWP

when accounting for all forcings. This difference is negligible in comparison to other uncertainties (see Table 3), and our GWP calculation therefore remains independent of box model results.

The indirect forcing from methane-induced changes to tropospheric ozone and stratospheric water vapour are determined by multiplying the calculated direct methane forcing (R_{CH4}) by scaling factors of 0.5 ± 55% and 0.15 ± 70% respectively (Myhre et al., 2013). Equivalent scaling factors from Forster et al., (2021) are 0.37 ± 50% and 0.106 ± 100%.

In addition to the methane-induced indirect radiative forcing from ozone and water vapour outlined above, we also consider non-methane induced forcing from H_2 as a source of tropospheric ozone and stratospheric water vapour. For stratospheric water vapour, the e-folding lifetime of the water vapour perturbation following a change in H_2, α_{H2O}, is derived from model spin-up data following a change to the H_2 lower boundary condition and is determined to be 8 years in the lower stratosphere. Values for both R_{H2O} and a_{H2O} are determined from the steady-state change in the stratospheric water profile between our UKESM1 BASE simulation and the simulation where the H_2 lower boundary condition is increased from 500 to 2000 ppb. A comparison of the vertical profile of stratospheric water vapour changes resulting from H_2 changes in our study (Figure 1d) with that resulting from methane changes between 1950 and 2000 in Figure 2b of Myhre et al. (2007), shows very similar H_2O changes at all altitudes. We therefore adopt the radiative forcing determined by Myhre et al. (2007) of 0.05 W m^{-2} with an estimated uncertainty of ±20% for stratospheric water vapour changes relative to base in our 2000H_2 UKESM1 scenario. This water vapour forcing is associated with a change of ~500 ppb in stratospheric water vapour at 30 km altitude, giving a value for R_{H2O} of 1×10^{-4} W m^{-2} (ppb H_2O)$^{-1}$ when considering changes at 30 km. We assume that the entire stratospheric H_2O profile will scale proportionally with the H_2 lower boundary condition (following results from our UKESM1 simulations using H_2 LBCs of 750, 1000, 1500 and 2000 ppb H_2), so the choice of 30 km for determining R_{H2O} is arbitrary. The production rate of water vapour per ppb change in H_2, a_{H2O}, can then be defined as the change in steady-state H_2O at 30 km (500 ppb) divided by the lifetime of 8 years and the change in H_2 mixing ratio of 1500 ppb.

For changes to the global mean tropospheric ozone column, the value for R_{O3} is 0.042 (0.037 to 0.047) W m^{-2} DU^{-1} and is taken directly from Myhre et al., (2013). No updated value for R_{O3} was presented in Forster et al. (2021), although a similar value of 0.039 W m^{-2} DU^{-1} can be derived based on the estimated change in tropospheric ozone of 109 ± 25 Tg between 1850 and 2005 and a stratospheric-temperature-adjusted radiative forcing due to tropospheric ozone of 0.39 ± 0.07 W m^{-2} between 1850 and 2010. The e-folding lifetime associated with the ozone perturbation, α_{O3}, is taken to be 0.07 years, calculated as the tropospheric O_3 burden divided by the loss in our UKESM1 base simulation. This is shorter than the lifetime used for the short-lived ozone perturbation in Fuglestvedt et al. (2010) of 0.267 years. However our results are insensitive to the difference between these values and small variations around them. The value for a_{O3} is calculated as the change in the steady-state global mean tropospheric ozone column in our 2000H_2 simulation relative to base (0.59 DU) divided by the lifetime of 0.07 years

and the change in H_2 mixing ratio of 1500 ppb. A list of all the input parameters with the values used in our AGWP calculations are presented in Table S1.

Changes in H_2 mixing ratio can also influence stratospheric ozone. In our UKESM1 simulations, the change in global mean stratospheric ozone column between our base and 2000H_2_CH4f (increased H_2, including the chemical feedback on the methane lifetime) scenarios was negligible at +0.10 DU, relative to a base value of 283.78 DU, and interannual variations of up to several DU. Based on a value for R for stratospheric ozone of 0.0054 W m^{-2} DU^{-1} (Schwarzkopf and Ramaswamy, 1993), and a range of e-folding lifetimes for the stratospheric ozone perturbation of between 1 and 10 years, this results in a GWP(100) of less than 0.03 using equations E1 to E4. We consider this to be below the uncertainty involved in the calculation and conclude that changes in stratospheric ozone for our range of scenarios do not significantly contribute to the hydrogen GWP.

For a 100 year time horizon we determine a H_2 GWP of 12 ± 6 (see Table 3). This value is larger than previously published studies which do not account for changes in stratospheric composition (Derwent et al., 2020, 5 ± 1, and Derwent and Field 2021, 3.3 ± 1.4), but similar to the values of Hauglustaine et al. (2022) (12.8 ± 5.2) and the multi-model study of Sand et al. (2023) (11.6 ± 2.8, one standard deviation) which include a tropospheric and stratospheric response. Approximately two thirds of our GWP arises from the influence of H_2 on methane and ozone distributions in the troposphere and one third from the influence of H_2 on stratospheric water vapour. Results from our study can also be compared with that of Paulot et al. (2021), who estimated the indirect radiative forcing at steady-state due to an increase in H_2. Their study accounted for changes in methane, tropospheric ozone and stratospheric water vapour and found an indirect radiative forcing arising from H_2 of 0.13 mW m^{-2} $ppb(H_2)^{-1}$. Using the radiative forcing scaling factors, we obtain a larger value of 0.18 ± 0.03 mW m^{-2} $ppb(H_2)^{-1}$ (the same value is obtained using both the Myhre et al., (2013) and Forster et al., (2021) radiative efficiency scaling factors), which may be partly explained by the larger methane feedback factor in UKESM1 (1.39) relative to the chemistry-climate model used in Paulot et al. (2021).

Uncertainties in our calculation are based on uncertainties in the hydrogen lifetime with respect to soil uptake, as well as uncertainties in radiative forcing scaling factors and the AGWP for CO_2. We do not account for uncertainties in chemical lifetimes and other UKESM1-derived quantities which are likely to vary when using different atmospheric models with different chemistry schemes. In addition, we also note that the sensitivity of ERF in UKESM1 to changes in methane is approximately 65% larger than that indicated by the radiative scaling factors used in the empirical relationships applied in the GWP calculation (O'Connor et al., 2022). This suggests a further source of uncertainty than accounted for by the radiative forcing scaling factor uncertainties outlined in Myhre et al. (2013) and Forster et al., (2021), associated with the response of both aerosols and clouds, as well as ozone and water vapour to changing methane levels.

Radiatively active species	H_2 GWP(100) IPCC AR5	H_2 GWP(100) IPCC AR6	H_2 GWP(20) IPCC AR5	H_2, GWP(20) IPCC AR6
Methane	4.7	5.2	13.4	14.7
Tropospheric ozone (methane and non-methane induced)	3.6	3.2	11.3	10.0
Total Troposphere	8.3	8.4	24.7	24.7
Stratospheric water vapour (methane and non-methane induced)	3.2	3.1	10.1	9.7
Total	11.5 (6 – 18)	11.5 (6 – 18)	34.8 (19 – 51)	34.4 (19 – 51)

Table 3. A comparison of the 100 and 20 year time horizon H_2 GWPs (GWP(100) and GWP(20) respectively) determined using radiative efficiencies and the AGWP for CO_2 from IPCC AR5 (Myhre et al., 2013) and from IPCC AR6 (Forster et al., 2021). Uncertainties quoted account for uncertainties in the H_2 lifetime with respect to soil uptake, radiative forcing scaling factors and the $AGWP_{CO2}$ only.

4 Discussion and conclusions

Leakage of hydrogen associated with a hydrogen economy will result in an indirect global warming, offsetting greenhouse gas emission reductions made as a result of a switch from fossil fuel to hydrogen. We have presented a methodology for calculating the indirect GWP of H_2, with principal contributions coming from changes in methane, in tropospheric ozone and in stratospheric water vapour. The GWP depends on the lifetime of H_2 in the atmosphere, on the perturbation lifetimes of the radiatively active species, (e.g., CH_4 and O_3) and on their effective production rates per unit change in H_2. We present values for these based on calculations with our chemistry-climate model, UKESM1 and a box model. The 100 year GWP for H_2, based on the above, is 12 ± 6, a value somewhat higher than some previous estimates, but similar to recent values from Hauglustaine et al. (2022) and Sand et al. (2023). Whilst our GWP uncertainty accounts for uncertainties associated with the size of the soil sink and radiative forcing scaling factors, it does not include uncertainties in model-derived parameters (e.g. chemical and perturbation lifetimes or the chemical production rates per unit change in H_2). In particular, uncertainties associated with the stratospheric response may be significant, as well as the response of aerosols and clouds to changing methane levels. Further simulations using different earth system models and different chemistry schemes would be required to fully assess the impact of uncertainties in these parameters on the hydrogen GWP.

Determining a GWP for hydrogen allows a change in hydrogen emissions to be compared to an equivalent change in carbon dioxide emissions in terms of time integrated radiative forcing. This increase in equivalent carbon dioxide emissions can be compared with expected reductions in carbon dioxide and methane (as equivalent CO_2) emissions to determine the net impact on radiative forcing. In our illustrative future global hydrogen economy scenario (Section 2.3) we estimate additional H_2 emissions of between 9 and 95 Tg H_2 yr^{-1}, based on a hydrogen economy supplying 23% of present day energy consumption and H_2 leakage rates of 1 and 10%. Using a H_2 GWP(100) of 12, this is equivalent to the time integrated radiative forcing from carbon dioxide emissions of about 110 and 1140 Tg CO_2 yr^{-1} respectively. Based on the fossil fuel energy sectors that are replaced by hydrogen, a low carbon method of hydrogen generation and the sector emissions described in Hoesly et al. (2018), we would expect a reduction in carbon dioxide emissions of ~26,000 Tg yr^{-1}. In addition a further reduction of ~1200 Tg yr^{-1} equivalent CO_2 emissions would result from expected methane emission reductions (assuming a GWP(100) for methane of 28), resulting in a total reduction of CO_2 equivalent emissions of ~27,200 Tg yr^{-1}. Therefore, in this global scenario the increase in equivalent CO_2 emissions based on 1% and 10% H_2 leakage rate offsets approximately 0.4 and 4% of the total equivalent CO_2 emission reductions respectively. Whilst the benefits from equivalent CO_2 emission reductions significantly outweigh the disbenefits arising from H_2 leakage, they clearly demonstrate the climate importance of controlling H_2 leakage within a hydrogen economy.

A switch to a hydrogen economy would also provide the opportunity to reduce emissions of other gases which can themselves directly or indirectly affect both climate and air quality. For example, an immediate impact of increased atmospheric H_2 is to reduce the concentration of OH, the major tropospheric oxidant, which would thus tend to increase the lifetime of methane. Increases in methane would adversely affect climate and also lead to production of tropospheric ozone, impacting both climate and air quality. However, we show that reductions in methane emissions associated with decreased fossil fuel use, along with reductions of CO and NO_x emissions, could lead to a net change in ozone close to (or below) zero with associated climate and air quality benefits, assuming very high H_2 leakage rates (e.g. scenario 2000H2_CH4f_O3pre, Figure 2j) and a green method of hydrogen production. In the case of no leakage of H_2, emission reductions in methane, CO, and NO_x lead to decreases in tropospheric ozone column globally (scenario 500H2, CH4f_O3pre, Figure 2h). To assess whether the ozone response to changes in emissions associated with a hydrogen economy is influenced by the assumed background climate conditions, (i.e. whether the timing of the implementation of a hydrogen economy could be important), we performed a set of additional model simulations using 2045-2055 climatological boundary conditions taken from the CMIP6-SSP2-4.5 scenario. These scenarios assumed a hydrogen economy of the same absolute size and identical leakage rates as our present day (2014) scenarios. We found no discernible difference in terms of the tropospheric and stratospheric ozone response to changes in H_2 and ozone precursors, with emission reductions from decreased fossil fuel use offering similar air quality benefits in both sets of simulations. To maximise the benefit of a switch to hydrogen, not only should hydrogen leakage be minimised, but the emissions of methane, CO, VOCs and NO_x should also be reduced to the maximum extent possible.

Author Contributions

JAP and ATA designed the research and supervised the analysis. JK performed the UKESM model simulations and atmospheric composition analysis and PTG and FMO performed the ERF calculations. KPS, JAP, PTG and NJW contributed to the H_2 GWP analysis. KPS derived the AGWP equations, with contributions from JAP. NJW performed the UKESM GWP calculations. All box modelling was performed by PTG. NJW compiled the emission changes for the different scenarios. All authors contributed to the writing of the manuscript.

Code availability

Due to intellectual property rights restrictions, we cannot provide either the source code or documentation papers for the UM. The Met Office Unified Model is available for use under licence. A number of research organisations and national meteorological services use the UM in collaboration with the Met Office to undertake basic atmospheric process research, produce forecasts, develop the UM code, and build and evaluate Earth system models. For further information on how to apply for a licence, see http://www.metoffice.gov.uk/research/modelling-systems/unified-model.

Acknowledgements

The research presented here was funded by the Department for Business, Energy and Industrial Strategy (BEIS). In addition, the HECTER project supported Alex Archibald, Paul Griffiths, Nicola Warwick (NE/X010236/1) and Keith Shine (NE/X010732/1) in the latter stages of this work. Fiona O'Connor was supported by the Met Office Hadley Centre Climate Programme, funded by BEIS. Model simulations and analysis were performed using Monsoon2, a collaborative High Performance Computing facility funded by the Met Office and the Natural Environment Research Council, JASMIN, the UK collaborative data analysis facility, and the NEXCS High Performance Computing facility funded by the Natural Environment Research Council and delivered by the Met Office. We thank Ken Caldeira and Lei Duan, Carnegie Institution for Science, for their contribution to the derivation of the AGWP equations. We also thank two anonymous reviewers, Matteo Bertagni, Princeton University, and Bill Collins, University of Reading, for useful comments that have helped improve the manuscript.

References

Alvarez, R.A., Zavala-Araiza, D., Lyon, D.R., Allen, D.T., Barkley, Z.R., Brandt, A.R., Davis, K.J., Herndon, S.C., Jacob, D.J., Karion, A. and Kort, E.A.: Assessment of methane emissions from the US oil and gas supply chain. Science, 361(6398), pp.186-188, 2018.

Archibald, A.T., Neu, J.L., Elshorbany, Y.F., Cooper, O.R., Young, P.J., Akiyoshi, H., Cox, R.A., Coyle, M., Derwent, R.G., Deushi, M. and Finco, A., et al.: Tropospheric Ozone Assessment Report: A critical review of changes in the tropospheric ozone burden and budget from 1850 to 2100. Elementa: Science of the Anthropocene, 8(1), 2020a.

Archibald, A. T., O'Connor, F. M., Abraham, N. L., Archer-Nicholls, S., Chipperfield, M. P., Dalvi, M., Folberth, G. A., Dennison, F., Dhomse, S. S., Griffiths, P. T., Hardacre, C., Hewitt, A. J., Hill, R. S., Johnson, C. E., Keeble, J., Köhler, M. O., Morgenstern, O., Mulcahy, J. P., Ordóñez, C., Pope, R. J., Rumbold, S. T., Russo, M. R., Savage, N. H., Sellar, A., Stringer, M., Turnock, S. T., Wild, O., and Zeng, G.: Description and evaluation of the UKCA stratosphere–troposphere chemistry scheme (StratTrop vn 1.0) implemented in UKESM1, Geosci. Model Dev., 13, 1223–1266, https://doi.org/10.5194/gmd-13-1223-2020, 2020b.

Bertagni, M.B., Pacala, S.W., Paulot, F. *et al.* Risk of the hydrogen economy for atmospheric methane. Nature Comms., 13, https://doi.org/10.1038/s41467-022-35419-7, 2022.

BP Energy Outlook, Energy Economics, https://www.bp.com/en/global/corporate/energy-economics.html, 2020.

Derwent, R. G., Collins, W. J., Johnson, C. E., and Stevenson, D. S.: Transient behaviour of tropospheric ozone precursors in a global 3D CTM and their indirect greenhouse effects, Climatic Change, 49, 463-487, 2001.

Derwent, R., Simmonds, P., O'Doherty, S., Manning, A., Collins, W., and Stevenson, D.: Global environmental impacts of the hydrogen economy, International Journal of Nuclear Hydrogen Production and Applications, 1(1), 57-67, 2006.

Derwent, R.G., Stevenson, D.S., Utembe, S.R., Jenkin, M.E., Khan, A.H. and Shallcross, D.E.: Global modelling studies of hydrogen and its isotopomers using STOCHEM-CRI: Likely radiative forcing consequences of a future hydrogen economy, International Journal of Hydrogen Energy, 45(15), pp.9211-9221, 2020.

E4tech, Ltd: H_2 emission potential review, BEIS Research Paper Number 22, 2019.

Ehhalt, D.H. and Rohrer, F.: The tropospheric cycle of H2: a critical review. *Tellus B: Chemical and Physical Meteorology*, *61*(3), pp.500-535, 2009.

Field, R.A. and Derwent, R.: Global warming consequences of replacing natural gas with hydrogen in the domestic energy sectors of future low-carbon economies in the United Kingdom and the United States of America, International Journal of Hydrogen Energy, 46, 30190-30203, 2021.

Forster, P., T. Storelvmo, K. Armour, W. Collins, J.-L. Dufresne, D. Frame, D.J. Lunt, T. Mauritsen, M.D. Palmer, M. Watanabe, M. Wild, and H. Zhang, 2021: The Earth's Energy Budget, Climate Feedbacks, and Climate Sensitivity. In *Climate Change 2021: The Physical Science Basis. Contribution of Working Group I to the Sixth Assessment Report of the Intergovernmental Panel on Climate Change* [Masson-Delmotte, V., P. Zhai, A. Pirani, S.L. Connors, C. Péan, S. Berger, N. Caud, Y. Chen, L. Goldfarb, M.I. Gomis, M. Huang, K. Leitzell, E. Lonn oy, J.B.R. Matthews, T.K. Maycock, T. Waterfield, O. Yelekçi, R. Yu, and B. Zhou (eds.)]. Cambridge University Press, Cambridge, United Kingdom and New York, NY, USA, pp. 923–1054, doi:10.1017/9781009157896.009, 2021.

Fuglestvedt, J. S., Shine, K. P., Berntsen, T., Cook, J., Lee, D. S., Stenke, A., Skeie, R. B., Velders, G. J. M., and Waitz, I. A.: Transport impacts on atmosphere and climate: Metrics, Atmos. Environ., 44, 4648–4677, 2010.

Frazer-Nash Consultancy: Fugitive hydrogen emissions in a future hydrogen economy, research paper for BEIS, https://www.gov.uk/government/publications/fugitive-hydrogen-emissions-in-a-future-hydrogen-economy, 2022.

Ghan, S. J.: Technical Note: Estimating aerosol effects on cloud radiative forcing, Atmos. Chem. Phys., 13, 9971–9974, https://doi.org/10.5194/acp-13-9971-2013, 2013.

Gidden, M. J., Riahi, K., Smith, S. J., Fujimori, S., Luderer, G., Kriegler, E., van Vuuren, D. P., van den Berg, M., Feng, L., Klein, D., Calvin, K., Doelman, J. C., Frank, S., Fricko, O., Harmsen, M., Hasegawa, T., Havlik, P., Hilaire, J., Hoesly, R., Horing, J., Popp, A., Stehfest, E., and Takahashi, K.: Global emissions pathways under different socioeconomic scenarios for use in CMIP6: a dataset of harmonized emissions trajectories through the end of the century, Geosci. Model Dev., 12, 1443–1475, https://doi.org/10.5194/gmd-12-1443-2019, 2019.

Grant, A., Archibald, A.T., Cooke, M.C., Nickless, G. and Shallcross, D.E.: Modelling the oxidation of 15 VOCs to track yields of hydrogen, Atmospheric Science Letters, 11(4), pp.265-269, 2010.

Hauglustaine, D., Paulot, F., Collins, W. et al.: Climate benefit of a future hydrogen economy, Commun. Earth Environ., 3, 295, https://doi.org/10.1038/s43247-022-00626-z, 2022.

Heimann, I., Griffiths, P. T., Warwick, N. J., Abraham, N. L., Archibald, A. T., & Pyle, J. A.: Methane emissions in a chemistry-climate model: Feedbacks and climate response, J. Adv. Model. Earth Sys., 12, e2019MS002019, https://doi.org/10.1029/2019MS002019, 2020.

Hoesly, R. M., Smith, S. J., Feng, L., Klimont, Z., Janssens-Maenhout, G., Pitkanen, T., Seibert, J. J., Vu, L., Andres, R. J., Bolt, R. M., Bond, T. C., Dawidowski, L., Kholod, N., Kurokawa, J.-I., Li, M., Liu, L., Lu, Z., Moura, M. C. P., O'Rourke, P. R., and Zhang, Q.: Historical (1750–2014) anthropogenic emissions of reactive gases and aerosols from the Community Emissions Data System (CEDS), Geosci. Model Dev., 11, 369–408, https://doi.org/10.5194/gmd-11-369-2018., 2018.

Jacobson, M. Z.: Effects of wind-powered hydrogen fuel cell vehicles on stratospheric ozone and global climate, Geophys. Res. Lett., 35, L19803, doi:10.1029/2008GL035102, 2008.

Kuhlbrodt, T., Jones, C. G., Sellar, A., Storkey, D., Blockley, E., Stringer, M., et al.: The low-resolution version of HadGEM3 GC3.1: Development and evaluation for global climate, Journal of Advances in Modeling Earth Systems, 10, 2865-2888, https://doi.org/10.1029/2018MS001370, 2018.

Lewis, A.C.: Optimising air quality co-benefits in a hydrogen economy: a case for hydrogen-specific standards for NO x emissions. *Environmental Science: Atmospheres*, *1*(5), pp.201-207, 2021.

Mulcahy, J. P., Johnson, C., Jones, C. G., Povey, A. C., Scott, C. E., Sellar, A., Turnock, S. T., Woodhouse, M. T., Abraham, N. L., Andrews, M. B., Bellouin, N., Browse, J., Carslaw, K. S., Dalvi, M., Folberth, G. A., Glover, M., Grosvenor, D. P., Hardacre, C., Hill, R., Johnson, B., Jones, A., Kipling, Z., Mann, G., Mollard, J., O'Connor, F. M., Palmiéri, J., Reddington, C., Rumbold, S. T., Richardson, M., Schutgens, N. A. J., Stier, P., Stringer, M., Tang, Y., Walton, J., Woodward, S., and Yool, A.: Description and evaluation of aerosol in UKESM1 and HadGEM3-GC3.1 CMIP6 historical simulations, Geosci. Model Dev., 13, 6383–6423, https://doi.org/10.5194/gmd-13-6383-2020, 2020.

Myhre, G., Nilsen, J. S., Gulstad, L., Shine, K. P., Rognerud, B., and Isaksen, I. S. A.: Radiative forcing due to stratospheric water vapour from CH_4 oxidation, Geophys. Res. Lett., 34, L01807, https://doi.org/10.1029/2006GL027472, 2007.

Myhre, G., D. Shindell, F.-M. Bréon, W. Collins, J. Fuglestvedt, J. Huang, D. Koch, J.-F. Lamarque, D. Lee, B. Mendoza, T. Nakajima, A. Robock, G. Stephens, T. Takemura and H. Zhang, 2013: Anthropogenic and Natural Radiative Forc- ing. In: *Climate Change 2013: The Physical Science Basis. Contribution of Working Group I to the Fifth Assessment Report of the Intergovernmental Panel on Climate Change* [Stocker, T.F., D. Qin, G.-K. Plattner, M. Tignor, S.K. Allen, J. Boschung, A. Nauels, Y. Xia, V. Bex and P.M. Midgley (eds.)]. Cambridge University Press, Cambridge, United Kingdom and New York, NY, USA, 2013.

Nisbet, E., Fisher, R., Lowry, D., France, J., Allen, G., Bakkaloglu, S., Broderick, T., Cain, M., Coleman, M., Fernandez, J., Forster, G., Griffiths, P., Iverach, C., Kelly, B., Manning, M., Nisbet-Jones, P., Pyle, J., Townsend-Small, A., Al-Shalaan, A., Warwick, N., and Zazzeri, G.: Methane mitigation: methods to reduce emissions, on the path to the Paris Agreement, Rev. Geophys., 58, e2019RG000675, https://doi.org/10.1029/2019rg000675, 2020.

Novelli, P. C., Lang, P. M., Masarie, K. A., Hurst, D. F., Myers, R., and Elkins, J. W.: Molecular hydrogen in the troposphere: Global distribution and budget, J. Geophys. Res., 104(D23), 30,427–30,444, 1999.

Ocko, I. B., and Hamburg, S. P.: Climate consequences of hydrogen emissions, Atmos. Chem. Phys., 22, 9349-9368, 2022.

O'Connor, F.M., Abraham, N.L., Dalvi, M., Folberth, G.A., Griffiths, P.T., Hardacre, C., Johnson, B.T., Kahana, R., Keeble, J., Kim, B., Morgenstern, O., Mulcahy, J.P., Richardson, M., Robertson, E., Seo, J., Shim, S., Teixeira, J.C., Turnock, S.T., Williams, J., Wiltshire, A.J., Woodward, S., and Zeng, G.: Assessment of pre-industrial to present-day anthropogenic climate forcing in UKESM1, Atmospheric Chemistry and Physics, 21, 1211–1243, 2021.

O'Connor, F. M., Johnson, B. T., Jamil, O., Andrews, T., Mulcahy, J. P., and Manners, J.: Apportionment of the pre-industrial to present-day climate forcing by methane using UKESM1: The role of the cloud radiative effect, Journal of Advances in Modeling Earth Systems, 14, e2022MS002991. https://doi.org/10.1029/2022MS002991, 2022.

Patterson, J. D., Aydin, M., Crotwell, A. M., and Saltzman, E. S.: H_2 in Antarctic firn air: Atmospheric reconstructions and implications for anthropogenic emissions, PNAS, 118 (36) e2103335118, https://doi.org/10.1073/pnas.2103335118, 2021.

Paulot, F., Paynter, D., Naik, V., Malyshev, S., Menzel, R. and Horowitz, L.W.: Global modeling of hydrogen using GFDL-AM4. 1: Sensitivity of soil removal and radiative forcing, International Journal of Hydrogen Energy, 46(24), 13446-13460, 2021.

Pieterse, G., Krol, M.C., Batenburg, A.M., M. Brenninkmeijer, C.A., Popa, M.E., O'doherty, S., Grant, A., Steele, L.P., Krummel, P.B., Langenfelds, R.L. and Wang, H.J.: Reassessing the variability in atmospheric H2 using the two-way nested TM5 model, Journal of Geophysical Research: Atmospheres, 118(9), 3764-3780, 2013.

Prather, M.J.: Lifetimes and eigenstates in atmospheric chemistry: Geophysical Research Letters, 21(9), 801-804, 1994.

Prather, M.J.: An environmental experiment with H_2?, Science, 302, 581-582, 2003.

Prather, M. J., Holmes, C. D., and Hsu, J.: Reactive greenhouse gas scenarios: Systematic exploration of uncertainties and the role of atmospheric chemistry, Geophys. Res. Lett., 39, L09803, https://doi.org/10.1029/2012GL051440, 2012.

Sand, M., Skeie, R.B., Sandstad, M. et al.: A multi-model assessment of the Global Warming Potential of hydrogen, Commun. Earth Environ. 4, 203, https://doi.org/10.1038/s43247-023-00857-8, 2023.

Saunois, M., Stavert, A. R., Poulter, B., Bousquet, P., Canadell, J. G., Jackson, R. B., Raymond, P. A., Dlugokencky, E. J., Houweling, S., Patra, P. K., Ciais, P., Arora, V. K., Bastviken, D., Bergamaschi, P., Blake, D. R., Brailsford, G., Bruhwiler, L., Carlson, K. M., Carrol, M., Castaldi, S., Chandra, N., Crevoisier, C., Crill, P. M., Covey, K., Curry, C. L., Etiope, G., Frankenberg, C., Gedney, N., Hegglin, M. I., Höglund-Isaksson, L., Hugelius, G., Ishizawa, M., Ito, A., Janssens-Maenhout, G., Jensen, K. M., Joos, F., Kleinen, T., Krummel, P. B., Langenfelds, R. L., Laruelle, G. G., Liu, L., Machida, T., Maksyutov, S., McDonald, K. C., McNorton, J., Miller, P. A., Melton, J. R., Morino, I., Müller, J., Murguia-Flores, F., Naik, V., Niwa, Y., Noce, S., O'Doherty, S., Parker, R. J., Peng, C., Peng, S., Peters, G. P., Prigent, C., Prinn, R., Ramonet, M., Regnier, P., Riley, W. J., Rosentreter, J. A., Segers, A., Simpson, I. J., Shi, H., Smith, S. J., Steele, L. P., Thornton, B. F., Tian, H., Tohjima, Y., Tubiello, F. N., Tsuruta, A., Viovy, N., Voulgarakis, A., Weber, T. S., van Weele, M., van der Werf, G. R., Weiss, R. F., Worthy, D., Wunch, D., Yin, Y., Yoshida, Y., Zhang, W., Zhang, Z., Zhao, Y., Zheng, B., Zhu, Q., Zhu, Q., and Zhuang, Q.: The Global Methane Budget 2000–2017, Earth Syst. Sci. Data, 12, 1561–1623, https://doi.org/10.5194/essd-12-1561-2020, 2020.

Schultz, M., Diehl, T., Brasseur, G. P. and Zittel, W.: Air pollution and climate-forcing impacts of a global hydrogen economy, Science, 302, 624-627, 2003.

Schwarzkopf, M. D. and Ramaswamy, Radiative forcing due to ozone in the 1980s: dependence on altitude of ozone change, Geophys. Res. Lett., 20, 205-208, 1993.

Sellar, A. A., Jones, C. G., Mulcahy, J., Tang, Y., Yool, A., Wiltshire, A., O'Connor, F. M., Stringer, M., Hill, R., Palmieri, J., Woodward, S., de Mora, L., Kuhlbrodt, T., Rumbold, S., Kelley, D. I., Ellis, R., Johnson, C. E., Walton, J., Abraham, N. L., Andrews, M. B., Andrews, T., Archibald, A. T., Berthou, S., Burke, E., Blockley, E., Carslaw, K., Dalvi, M., Edwards, J., Folberth, G. A., Gedney, N., Griffiths, P. T., Harper, A. B., Hendry, M. A., Hewitt, A. J., Johnson, B., Jones, A., Jones, C. D., Keeble, J., Liddicoat, S., Morgenstern, O., Parker, R. J., Predoi, V., Robertson, E., Siahaan, A., Smith, R. S., Swaminathan, R., Woodhouse, M. T., Zeng, G., and Zerroukat, M.: UKESM1: Description and evaluation of the UK Earth System Model, J. Adv. Model. Earth Sy., 11, 4513–4558, https://doi.org/10.1029/2019ms001739, 2020.

Staffell, I., Scamman, D., Abad, A.V., Balcombe, P., Dodds, P.E., Ekins, P., Shah, N. and Ward, K.R.: The role of hydrogen and fuel cells in the global energy system, Energy & Environmental Science, 12(2), 463-491, 2019.

Stevenson, D. S., Young, P. J., Naik, V., Lamarque, J.-F., Shindell, D. T., Voulgarakis, A., Skeie, R. B., Dalsoren, S. B., Myhre, G., Berntsen, T. K., Folberth, G. A., Rumbold, S. T., Collins, W. J., MacKenzie, I. A., Doherty, R. M., Zeng, G., van Noije, T. P. C., Strunk, A., Bergmann, D., Cameron-Smith, P., Plummer, D. A., Strode, S. A., Horowitz , L., Lee, Y. H., Szopa, S., Sudo, K., Nagashima , T., Josse, B., Cionni, I., Righi, M., Eyring, V., Conley, A., Bowman, K. W., Wild, O., and Archibald, A.: Tropospheric ozone changes, radiative forcing and attribution to emissions in the Atmospheric Chemistry and Climate Model Intercomparison Project (ACCMIP), Atmos. Chem. Phys., 13, 3063–3085, https://doi.org/10.5194/acp-13-3063-2013, 2013.

Stevenson, D. S., Zhao, A., Naik, V., O'Connor, F. M., Tilmes, S., Zeng, G., Murray, L. T., Collins, W. J., Griffiths, P. T., Shim, S., Horowitz, L. W., Sentman, L. T., and Emmons, L.: Trends in global tropospheric hydroxyl radical and methane lifetime since 1850 from AerChemMIP, Atmos. Chem. Phys., 20, 12905–12920, https://doi.org/10.5194/acp-20-12905-2020, 2020.

Tromp. T. K., Shia, R.-L., Allen, M., Eiler, J. and Yung, Y. L.: Potential environmental impact of hydrogen on the stratosphere, Science, 300, 1740-1742, 2003.

Warwick, N.J., Bekki, S., Nisbet, E.G. and Pyle, J.A.: Impact of a hydrogen economy on the stratosphere and troposphere studied in a 2-D model, Geophysical Research Letters, 31(5), 2004.

Warwick, N. J., Griffiths, P. T., Keeble, J., Archibald, A. T., Pyle, J. A., and Shine, K., Atmospheric implications of increased hydrogen use, research paper for BEIS, https://www.gov.uk/government/publications/atmospheric-implications-of-increased-hydrogen-use, 2022.

Williams, K.D., Copsey, D., Blockley, E.W., Bodas-Salcedo, A., Calvert, D., Comer, R., Davis, P., Graham, T., Hewitt, H.T., Hill, R. and Hyder, P.: The Met Office global coupled model 3.0 and 3.1 (GC3. 0 and GC3. 1) configurations, Journal of Advances in Modeling Earth Systems, 10(2), pp.357-380. 2018.

Zheng, B., Chevallier, F., Yin, Y., Ciais, P., Fortems-Cheiney, A., Deeter, M. N., Parker, R., Wang, Y., Worden, H. and Zhao, Y.: Global atmospheric carbon monoxide budget 2000-2017 inferred from multi-species atmospheric inversions, Earth Syst. Sci. Data, 11, 1411-1436, 2019.